The Plant Cell, Vol. 27: 2677–2691, October 2015, www.plantcell.org

BREAKTHROUGH REPORT

Discovery of a Unique Clp Component, ClpF, in Chloroplasts: A Proposed Binary ClpF-ClpS1 Adaptor Complex Functions in Substrate Recognition and Delivery[OPEN]

Kenji Nishimura,[a,1] Janina Apitz,[c] Giulia Friso,[a] Jitae Kim,[a] Lalit Ponnala,[b] Bernhard Grimm,[c] and Klaas J. van Wijk[a,2]

[a] Department of Plant Biology, Cornell University, Ithaca, New York 14853
[b] Computational Biology Service Unit, Cornell University, Ithaca, New York 14853
[c] Department of Plant Physiology, Humboldt University, 10115 Berlin, Germany

ORCID ID: 0000-0001-9536-0487 (K.J.v.W.)

Clp proteases are found in prokaryotes, mitochondria, and plastids where they play crucial roles in maintaining protein homeostasis (proteostasis). The plant plastid Clp machinery comprises a hetero-oligomeric ClpPRT proteolytic core, ATP-dependent chaperones ClpC and ClpD, and an adaptor protein, ClpS1. ClpS1 selects substrates to the ClpPR protease-ClpC chaperone complex for degradation, but the underlying substrate recognition and delivery mechanisms are currently unclear. Here, we characterize a ClpS1-interacting protein in *Arabidopsis thaliana*, ClpF, which can interact with the Clp substrate glutamyl-tRNA reductase. ClpF and ClpS1 mutually stimulate their association with ClpC. ClpF, which is only found in photosynthetic eukaryotes, contains bacterial uvrB/C and YccV protein domains and a unique N-terminal domain. We propose a testable model in which ClpS1 and ClpF form a binary adaptor for selective substrate recognition and delivery to ClpC, reflecting an evolutionary adaptation of the Clp system to the plastid proteome.

INTRODUCTION

Intracellular proteolysis is essential for proteome dynamics and homeostasis (proteostasis). Macromolecular proteolytic machineries, such as the Clp proteases and the 26S proteasome, play a pivotal role in proteostasis. ATP-dependent Clp proteases are present in bacteria and eukaryotic organelles of bacterial origin, namely, mitochondria and plastids, where they regulate a broad range of substrates (Sauer and Baker, 2011; Alexopoulos et al., 2012; Liu et al., 2014; Nishimura and van Wijk, 2015). Clp proteases consist of ATP-dependent chaperones that form hexameric rings, i.e., AAA+ (ATPases associated with diverse cellular activities) chaperones, which associate with a barrel-shaped tetradecameric protease core complex. Substrates are unfolded by these chaperone rings and are then directly delivered into the Clp protease core. To ensure optimal levels of functional proteins and to remove aggregated, misfolded, or otherwise damaged proteins while avoiding uncontrolled degradation, substrate recognition and delivery are tightly regulated. To this end, bacterial Clp proteases use adaptor proteins such as ClpS and destabilizing signals in the N-terminal, C-terminal, or internal regions of proteins (known as degrons) (Kirstein et al., 2009; Battesti and Gottesman, 2013). Degradation of N-terminal degrons (N-degrons) is conceptualized in the N-end rule, which relates the stability of a protein to the identity of its N-terminal amino acid residue (Varshavsky, 2011; Dougan et al., 2012). In addition, many bacteria employ a specialized 11-amino acid SsrA peptide tag, which is added to the C terminus of nascent proteins from a specific mRNA during stalled translation. The adaptors select substrates through their degrons and deliver them to the Clp chaperones, but the adaptors can also indirectly influence the affinity of the Clp chaperones (Battesti and Gottesman, 2013).

Escherichia coli ClpS recognizes substrates containing N-degrons and delivers them to the chaperone's N-terminal domain (N-domain) for degradation (Erbse et al., 2006; Rivera-Rivera et al., 2014). The ClpS core domain is responsible for substrate recognition and N-domain docking (Zeth et al., 2002; Erbse et al., 2006). The substrate delivery into the Clp protease core complex is triggered by ClpA pulling on an unstructured N-terminal extension (NTE) of ClpS (Rivera-Rivera et al., 2014). Notably, ClpS is necessary and sufficient for recognition and delivery of N-end substrates in the bacterial Clp system, without any known additional factors. *E. coli* ClpS inhibits the ClpAP-mediated degradation of SsrA-tagged proteins and of ClpA itself (Dougan et al., 2012).

The structure and action mechanisms of the Clp machinery have diversified during evolution (Nishimura and van Wijk, 2015). Plant chloroplasts harbor the most complex Clp system, consisting of a hetero-oligomeric protease core comprising five proteolytically active subunits (ClpP1 and ClpP3 to ClpP6) and four proteolytically inactive proteins (ClpR1 to ClpR4), as well as two stabilizing/activating factors (ClpT1/2), three AAA+ chaperones (ClpC1, ClpC2, and ClpD), and the adaptor ClpS1 (Nishimura and van Wijk, 2015). Multiple substrate degradation pathways

[1] Current address: Institute of Plant Science and Resources, Okayama University, Kurashiki 710-0046, Okayama, Japan.
[2] Address correspondence to kv35@cornell.edu.
The author responsible for distribution of materials integral to the findings presented in this article in accordance with the policy described in the Instructions for Authors (www.plantcell.org) is: Klaas J. van Wijk (kv35@cornell.edu).
[OPEN]Articles can be viewed online without a subscription.
www.plantcell.org/cgi/doi/10.1105/tpc.15.00574

involving plastid Clp protease have been proposed (Nishimura and van Wijk, 2015). The stability of bacterial ClpA depends on the presence of ClpS (Dougan et al., 2002), but ClpC stability in chloroplasts is independent of ClpS1 (Nishimura et al., 2013). SsrA sequences have not been found in plastid genomes, implying the absence of this tagging system in plastids. Nonetheless, ClpS1 physically interacts with ClpC1/2 and recognizes a subset of proteins, such as glutamyl tRNA reductase 1 (GluTR1; also known as HEMA1, AT1G58290) (Nishimura et al., 2013). Importantly, we recently obtained tentative evidence that in vivo degradation of GluTR1 requires the ClpC chaperones and the ClpPR core and that ClpS1 is involved in this degradation (J. Apitz, K. Nishimura, A. Wolf, B. Hedtke, K.J. van Wijk, and B. Grimm, unpublished data). On the other hand, the chloroplast copper transporter PAA2 was recently shown to be an in vivo substrate for the chloroplast Clp system involving both ClpC and the ClpPR core, but this degradation is independent of ClpS1 (Tapken et al., 2015).

ClpS1 affinity studies aiming at isolating ClpS1 substrates also identified a protein (AT2G03390) that we initially named UVR (Nishimura et al., 2013). Unlike other ClpS1 interactors, the interaction between ClpS1 and UVR does not depend on the conserved substrate binding residues (D89/N90) in the core domain of ClpS1 (Nishimura et al., 2013). This prompted us to hypothesize that UVR might not be a substrate, but rather it may interact with ClpS1 for regulatory reasons. Here, we show that UVR interacts with both ClpS1 and the chaperones ClpC1 and ClpC2, and we propose that it is a novel adaptor protein within the Clp system. We renamed this protein ClpF, indicating that it is part of the chloroplast Clp system. ClpF can interact with the Clp substrate GluTR1 (hereafter referred to as GluTR), and we propose a model in which ClpF, together with ClpS1, delivers GluTR to ClpC chaperones. ClpF and ClpS1 mutually stimulate their interaction with the ClpC1/2 chaperones, as observed by in vitro assays. Our data suggest that ClpS1 and ClpF may form a binary adaptor complex in plastids; we propose a noncanonical substrate recognition and delivery mechanism requiring this ClpS1-ClpF binary adaptor system.

RESULTS

ClpF Has a Tripartite Mosaic Structure Conserved across Photosynthetic Eukaryotes

Primary sequence and structural modeling analyses suggest that ClpF comprises an N-terminal chloroplast targeting sequence (amino acids 1 to 65) and three distinct domains: (1) an N-terminal domain (amino acids 66 to 138) with unknown function, which we designated as NTD; (2) a uvrB/C motif (amino acids 153 to 188); and (3) a YccV-like domain (amino acids 203 to 310) in the C terminus (Figure 1A). Homology modeling (Figure 1A) suggests that NTD and uvrB/C motif helices are aligned in an antiparallel orientation in front of the YccV-like domain. The uvrB/C motif was originally found as a homologous region of ~35 amino acids that is shared in two DNA excision repair proteins, UvrB and UvrC, involved in recognition and processing of damaged DNA in proteobacteria (Moolenaar et al., 1995). YccV proteins are found across multiple prokaryotes, and YccV-like domains are found in combination with various other functional domains in eukaryotes, including cysteine proteases and various metabolic enzymes (http://supfam.org). The YccV protein HspQ (heat shock protein Q) in *E. coli* stimulates degradation of a subset of denatured proteins in an unknown fashion (Shimuta et al., 2004), and it was also suggested to be a hemimethylated DNA binding protein influencing the stability of a replication initiation protein (d'Alencon et al., 2003).

Homologs of *Arabidopsis thaliana* ClpF are present in green algae, the moss *Physcomitrella patens*, and angiosperms, but not in non-green algae, cyanobacteria or nonphotosynthetic organisms. Phylogenetic analysis of ClpF proteins from three green algal species, moss, and 28 angiosperms showed that ClpF homologs are separated into different clades according to the green lineage (Figure 1B). The subclades for monocots and dicots indicate a significant diversification within angiosperms. Most plant species examined contain a single ClpF protein, but rice (*Oryza sativa*) (monocotyledon) and soybean (*Glycine max*) (dicotyledon) each possess two paralogs. Importantly, direct homologs of bacterial UvrB/C or YccV proteins are not found in these ClpF containing species. Thus, the tripartite mosaic structure of ClpF appears to have been generated through genomic rearrangement accompanied with horizontal gene transfer from ancient cyanobacterial to eukaryotic nuclear genomes during endosymbiosis.

ClpF Is Localized in Chloroplasts and Is Constitutively Expressed in Green Tissues

We previously identified the (acetylated) ClpF N terminus starting with Arg-69 in ClpS1 pull-down assays with stromal proteome of isolated chloroplasts, supporting chloroplast localization (Nishimura et al., 2013). Biochemical analysis using a specific ClpF antibody confirmed that ClpF is chloroplast-localized, with the majority located in the soluble stromal fraction and the remainder associated with chloroplast membranes (Figure 1C). We did not find ClpF in isolated chloroplast nucleoid fractions in Arabidopsis (Huang et al., 2013), indicating that its role is unlikely to be involved in DNA repair or plastid gene expression. To assess the spatiotemporal regulation of ClpF abundance, its accumulation was determined in different leaf stages and organs of Arabidopsis plants grown on soil (Figure 1D). ClpF was present throughout all leaf developmental stages examined, with a slight reduction during senescence. ClpF also accumulated in stems and flowers, and its level was relatively low in siliques. These observations indicate that ClpF expression is constitutive in photosynthetic tissues but is influenced by leaf development and organ differentiation. Similar protein accumulation patterns were observed for the ClpPR core (using ClpP6 as a representative) and ClpC1 (Figure 1D). More prominent changes in the protein levels during leaf expansion and senescence were found for ClpS1 and ClpC2 (Figure 1D). Publicly available *CLPF* mRNA expression data (http://bar.utoronto.ca/efp/cgi-bin/efpWeb.cgi) are consistent with ClpF protein accumulation data and show predominant expression in cotyledons, leaves, cauline leaves, and petals.

Loss-of-Function ClpF Mutants

We obtained two Arabidopsis T-DNA insertion lines for the *CLPF* gene, with T-DNA insertions located in the sixth exon (*clpf-1*) and

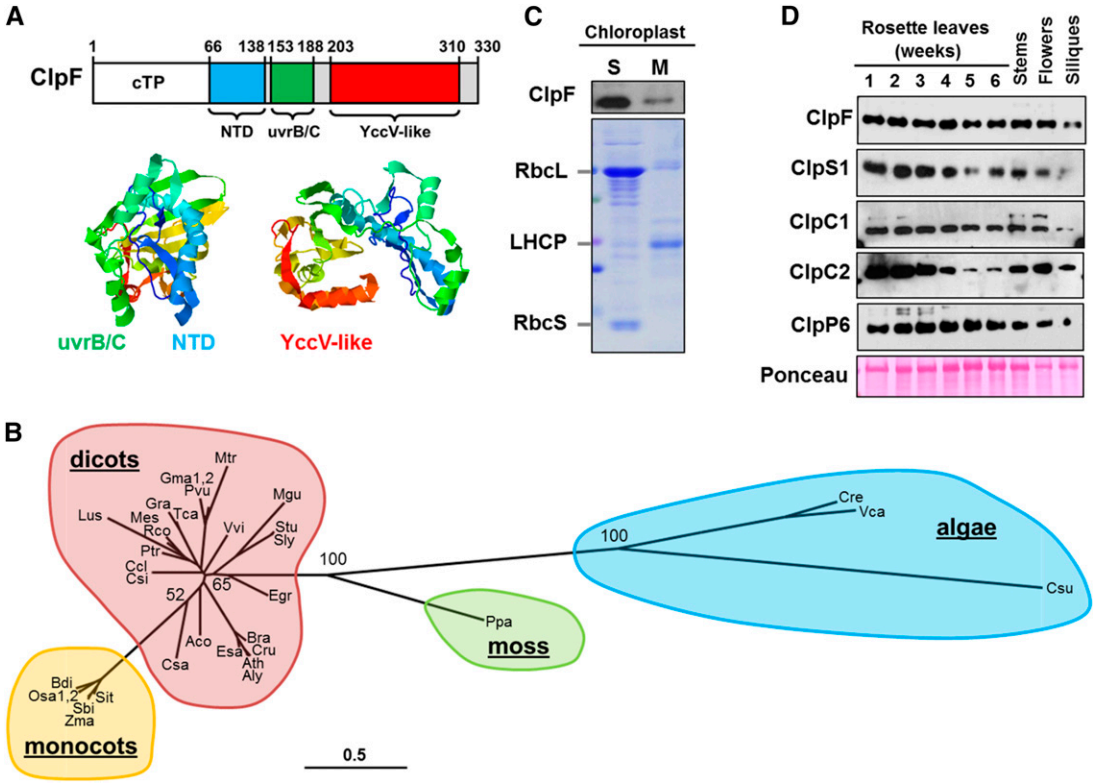

Figure 1. Primary Sequence Organization, Structural Homology Model, Phylogeny, Localization, and Expression of ClpF.

(A) ClpF primary sequence organization and structural model (AT2G03390). Following the N-terminal chloroplast transit peptide (cTP; amino acids 1 to 65), ClpF has a unique N-terminal domain (NTD), and uvrB/C and YccV-like domains. The latter domains are derived from different bacterial proteins that are missing in photosynthetic eukaryotes.

(B) BLAST searches followed by phylogenetic analysis of ClpF proteins shows the exclusive presence in photosynthetic eukaryotes, divided into four clades for monocotyledonous and dicotyledonous angiosperms, the moss *P. patens*, and green algae. RAxML bootstrap support values (>50) are indicated. Ath, *Arabidopsis thaliana*; Ppa, *Physcomitrella patens*; Sit, *Setaria italic*; Sbi, *Sorghum bicolor*; Zma, *Zea mays*; Bdi, *Brachypodium distachyon*; Osa, *Oryza sativa*; Mgu, *Mimulus guttatus*; Csa, *Cucumis sativus*; Stu, *Solanum tuberosum*; Sly, *Solanum lycopersicum*; Lus, *Linum usitatissimum*; Egr, *Eucalyptus grandis*; Mtr, *Medicago truncatula*; Gma, *Glycine max*; Pvu, *Phaseolus vulgaris*; Bra, *Brassica rapa*; Esa, *Eutrema salsugineum*; Cru, *Capsella rubella*; Aly, *Arabidopsis lyrata*; Aco, *Aquilegia coerulea*; Vvi, *Vitis vinifera*; Gra, *Gossypium raimondii*; Tca, *Theobroma cacao*; Csi, *Citrus sinensis*; Ccl, *Citrus clementina*; Ptr, *Populus trichocarpa*; Rco, *Ricinus communis*; Mes, *Manihot esculenta*; Csu, *Coccomyxa subellipsoidea*; Vca, *Volvox carteri*; Cre, *Chlamydomonas reinhardtii.*

(C) Localization of ClpF in chloroplasts. Chloroplast stroma and membranes were isolated from wild-type leaves and analyzed by SDS-PAGE followed by immunoblotting with anti-ClpF antibody (upper panel). Each lane contains 10 µg of the proteins. The Coomassie blue-stained gel is shown in the lower panel. S, chloroplast stroma; M, total chloroplast membranes.

(D) Protein accumulation levels of Clp components ClpF, ClpS1, ClpC1, ClpC2, and ClpP6 in rosette leaves of different ages, stems, flowers, and siliques. Total proteins (10 µg for ClpF and ClpP6; 20 µg for ClpS1 and ClpC1/2) extracted from the indicated organs were separated by SDS-PAGE and analyzed by immunoblotting with the specific antibodies. A portion of the Ponceau-stained membrane is shown as the loading control.

fourth exon (*clpf-2*) (Figures 2A and 2B). RT-PCR and immunoblot analyses showed a complete loss of *CLPF* transcript and ClpF protein (Figure 2C). The *clpf* plants were visibly indistinguishable from the wild type, which was similar to *clps1* (Figure 2B) but distinct from the pale-green or embryo lethal phenotypes of ClpPR core, *clpc1*, or *clpt1 clpt2* double mutants (Kim et al., 2009, 2013, 2015; Nishimura et al., 2013). We then generated a *clpf-1 clps1* double null mutant, which did not show a visible phenotype either (Figure 2B). However, careful determination of chlorophyll and carotenoid levels of leaf rosettes of young seedlings (stage 1.07) showed a 10% loss of total chlorophyll on fresh weight basis for the *clps1*, *clpf-1*, and double mutant, as well as a 4 to 7% increase in chlorophyll *a*/*b* ratio and 4 to 8% decreased levels of chlorophyll-to-carotenoid ratios (Supplemental Data Set 1), suggesting limited but significant defects in chloroplast functions. Interestingly, immunoblot analysis showed that ClpS1, but not other Clp subunits (ClpC1, C2, P6, or R2), overaccumulated >3-fold in isolated chloroplast stroma from *clpf-1* (Figure 2C). ClpS1 protein overaccumulation was not due to upregulation of *CLPS1* gene expression, since the *CLPS1* mRNA level in *clpf-1* was similar to that in the wild type (Figure 2C). We note that ClpS1 also overaccumulated (~3-fold) in the *clpc1* null mutant (Nishimura et al., 2013). In contrast, ClpF levels slightly decreased in *clps1*, *clpc2*, and *clps1 clpc2* double null mutants but increased in the *clpc1* null mutant (Figure 2D). This is consistent with the dominance of ClpC1 compared with

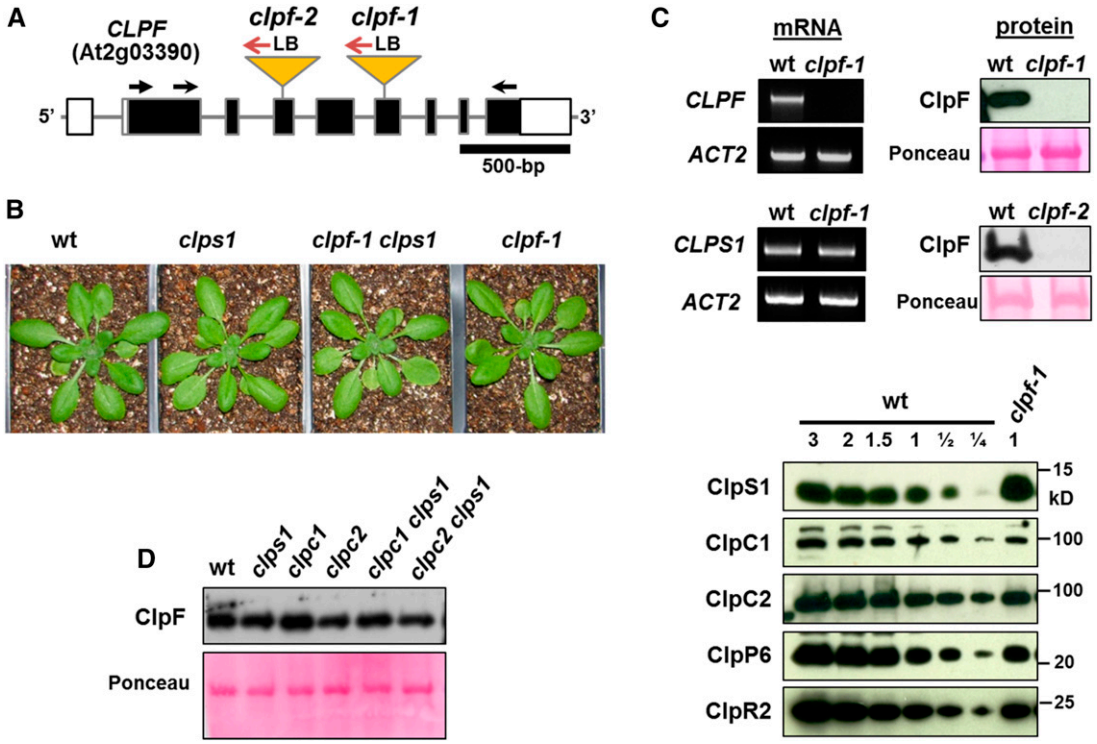

Figure 2. Identification and Characterization of *clpf* Null Mutants.

(A) Gene model and position of T-DNA insertions in the *clpf* null mutants. Exons (black boxes in the coding sequence), 5′ and 3′ untranslated regions (open boxes), and T-DNA insertions (triangles) are indicated. Arrows indicate primers used for genotyping or RT-PCR. LB, left-hand border.
(B) The wild type, *clpf-1*, *clps1*, and the double mutant *clpf-1 clps1* grown on soil for 24 d under a 10-h/14-h light/dark cycle at 120 µmol photons m^{-2} s^{-1}.
(C) RT-PCR based *CLPF* and *CLPS1* mRNA accumulation (indicated as mRNA) and Clp protein accumulation in the *clpf* alleles. For RT-PCR analysis, *ACTIN2* (*ACT2*) gene serves as normalization control for mRNA level. Primers are listed in Supplemental Data Set 4. For immunoblot analysis of ClpF accumulation, total leaf proteins were extracted from wild-type and *clpf* null alleles, and equal amounts of the proteins were loaded in each lane (20 µg for upper panels and 15 µg for lower panels) and analyzed by immunoblotting with the specific antibody. A portion of the Ponceau-stained membrane is shown as the loading control. For immunoblotting of accumulation of the other Clp subunits, equal amounts or the indicated dilutions (1× = 20 µg) of total leaf proteins from the wild type and *clpf-1* were analyzed using antibodies raised against ClpS1, ClpC1, ClpC2, ClpP6, and ClpR2. ClpS1 accumulation level is more than 3-fold higher in *clpf-1*.
(D) ClpF levels in the wild type and the homozygous null alleles *clps1*, *clpc1*, *clpc2*, and respective *clps1 clpc1* and *clps1 clpc2* double mutants. Twenty micrograms of total leaf proteins extracted from the indicated genotypes was subjected to immunoblot analysis with anti-ClpF antibody. Ponceau-stained membrane is shown as the loading control.

ClpC2, the strong growth and biochemical phenotypes of *clpc1*, and the lack of phenotype of *clpc2* (Nishimura and van Wijk, 2015).

To further characterize the *clpf* mutants, we performed a comparative, quantitative stromal proteome analysis of soil-grown wild-type, *clpf-1*, and *clps1* rosette leaves (three biological replicates) using label-free spectral counting by tandem mass spectrometry (MS/MS). This identified 733 chloroplast proteins (Supplemental Data Set 2). Principle component analysis suggested a measurable proteome phenotype for the mutants (Figure 3A). In addition to proteins involved in various metabolic functions, proteins related to chloroplast protein homeostasis were well represented with some 160 proteins, including 21 tRNA synthetases, 71 plastid ribosomal proteins and translation factors, 19 chaperones/protein isomerases, and 23 peptidases (Supplemental Data Set 2). Comparison of the chloroplast stromal protein mass investments across 28 identified functions between the genotypes showed little phenotypic difference. At the individual protein level and following stringent statistical significance analysis ($P < 0.01$ and false discovery rate < 0.05), there were 12 upregulated and 12 downregulated proteins in *clpf-1* compared with the wild type, and three and seven up- and down-regulated proteins, respectively, in *clps1*; six of these differentially expressed proteins in *clps1* were also significantly affected in *clpf-1* (Supplemental Data Set 3). Proteins in *clps1* generally responded in the same direction (up/down) as in *clpf*, with the exception of a pair of histidinol-phosphate aminotransferases with unknown functions that were not detected in *clps1* (Supplemental Data Set 3). The up- or downregulated proteins were distributed across multiple stromal functions, without a particular functional enrichment. These observations suggest that ClpF mainly functions together with ClpS1 in maintaining the abundance of a limited number of plastid proteins and in fine-tuning substrate selection for the Clp system.

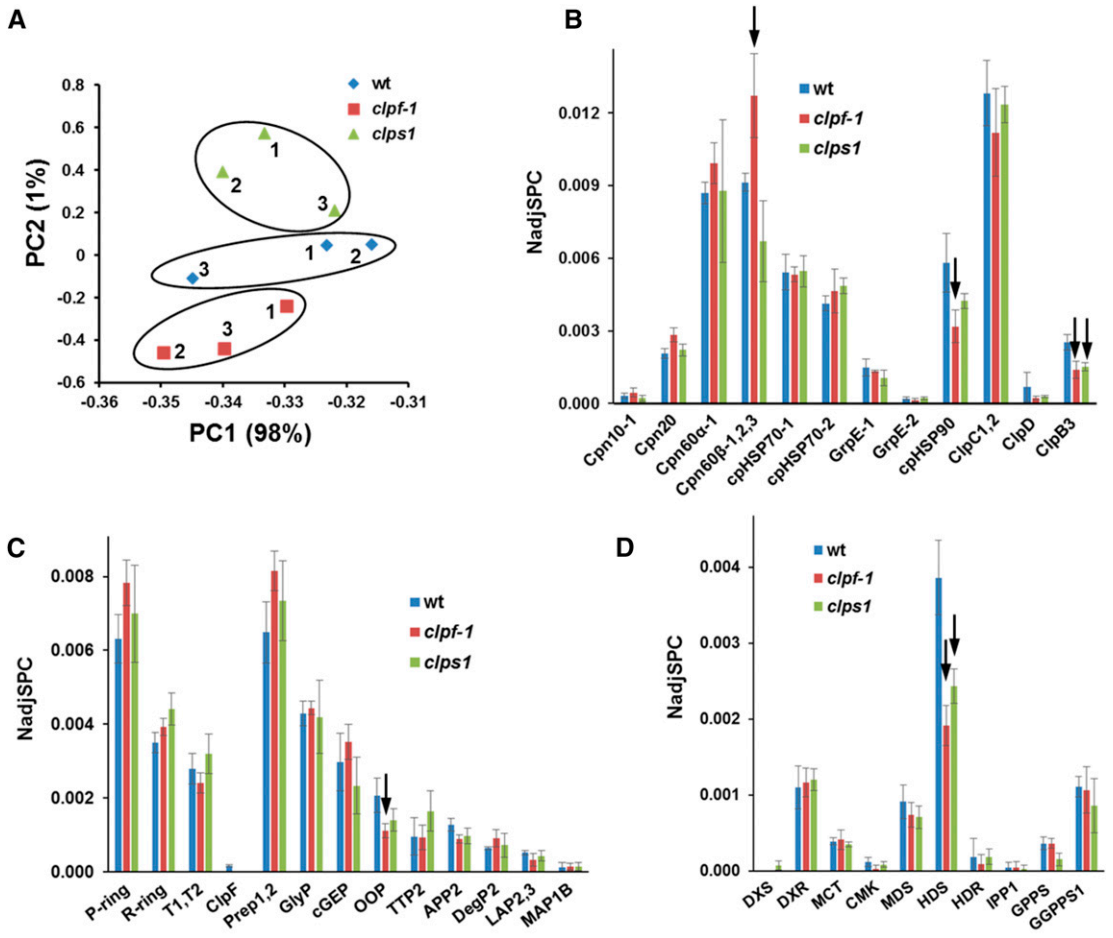

Figure 3. Comparative Quantitative Proteomics of Soil-Grown Plants for *clpf-1*, *clps1*, and the Wild Type.

Protein abundances were quantified based on the number of matched adjusted MS/MS spectra (NadjSPC). The spectral counting experiments identified 733 chloroplast proteins (Supplemental Data Set 3A), representing 95% of the total adjSPC, indicative of highly purified chloroplasts.
(A) Principal component analysis based on NadjSC of individual replicates for the three genotypes.
(B) to **(D)** Accumulation of chloroplast stromal chaperones **(B)**, peptidases **(C)**, and enzymes of the MEP pathway **(D)** in the three genotypes. Bars indicate standard deviations ($n = 3$). Arrows indicate proteins with statistically significant differences in abundance ($P < 0.01$ and <5% FDR). Whereas not statistically significant, CPN10, CPN20, and CPN60α levels were also commonly higher in *clpf-1* compared with *clps1* and the wild type, but levels of HSP70 and its ADP exchangers GrpE1,2 did not increase in *clpf-1*.

Interestingly, both ClpB3 and HSP90 were significantly downregulated in *clpf* and *clps1* (Supplemental Data Set 3). This is striking because both chaperones are strongly (up to ~10-fold) upregulated in the ClpC, ClpT, and ClpPR mutants (Nishimura and van Wijk, 2015). Furthermore, CPN60-β family chaperone proteins were significantly upregulated in *clpf-1* but not in *clps1*. We therefore plotted the quantitative response of all plastid chaperones and peptidases for the three genotypes (Figures 3B and 3C). Out of the various peptidases quantified, only the OOP peptidase was significantly affected (nearly 2-fold reduced levels) in *clpf-1* (Figure 3C; Supplemental Data Set 3). This M3 peptidase is thought to degrade cleavage products from upstream proteases, such as the Clp system or Prep1,2 (Kmiec et al., 2013; Nishimura and van Wijk, 2015).

The 2-C-methyl-D-erythritol 4-phosphate/1-deoxy-D-xylulose 5-phosphate (MEP) pathway provides the isoprenoids in plastids needed for the biosynthesis of carotenoids and the phytyl moiety of chlorophylls, quinines, and tocopherols; this pathway is essential and tightly regulated at both the transcriptional and posttranscriptional levels (Banerjee and Sharkey, 2014; Rodríguez-Concepción and Boronat, 2015). The MEP pathway enzyme 4-hydroxy-3-methylbutyl diphosphate synthase (HDS) was found to be strongly upregulated (2- to 10-fold) in *clpc1*, *clpt1 clpt2* double mutants, and ClpPR mutants (Kim et al., 2009, 2015; Zybailov et al., 2009; Nishimura et al., 2013). Here, we evaluated the quantitative response of the MEP pathway in *clpf-1* compared with the wild type and *clps1* (Figure 3D). We identified all seven steps in the pathway, as well as the IPP1, GPPS, and GGPPS enzymes immediately downstream of the MEP pathway. Interestingly, only HDS was significantly (~2-fold) downregulated in both *clpf* and *clps1*; this is precisely the

opposite response to that in the ClpC, P, R, and T mutants (see Discussion).

ClpF Interacts with ClpS1 through Its NTD

Previously we showed that endogenous stromal ClpF interacts with recombinant ClpS1 (Nishimura et al., 2013). To test the in vivo interaction between ClpF and ClpS1, we performed coimmunoprecipitations (co-IPs) using ClpF antibody (Figure 4A). ClpS1 was detected in the co-IP of wild-type protein extracts but not of *clpf-1*, demonstrating that indeed ClpF interacts with ClpS1 in vivo. In contrast, ClpC1/2 did not coimmunoprecipitate with ClpF (Figure 4A). MS/MS analysis of such co-IPs did not identify other proteins that were significantly enriched with ClpF. To further probe the physical interaction between ClpF and ClpS1, in vitro pull-down experiments were performed using recombinant His-tagged ClpF and glutathione *S*-transferase (GST)-fused wild-type and double alanine mutant ClpS1 protein (D89A/N90A) (Figure 4B). ClpF coeluted with both wild-type and mutant ClpS1, confirming their direct interaction, independent of the conserved ClpS1 substrate binding residues located in the ClpS1 core. ClpS1 consists of two separate domains (the NTE and core) (Figure 4C). In vitro pull-down assays using GST-ClpF and His-tagged ClpS1 lacking NTE showed that the ClpS1 core is sufficient for its ClpF interaction (Figure 4D). We then examined which domains in ClpF are responsible for the ClpS1 interaction. Based on the structural model (Figure 1A), we created three GST fusions for the different ClpF domains (NTD, uvrB/C, and YccV-like; Figure 4C) followed by in vitro pull-down assays using His-tagged ClpS1. ClpS1 copurified with full-length ClpF, and to a lesser degree with the ClpF NTD, but not with the individual uvrB/C or YccV domains (Figure 4E). This indicates that the ClpF NTD serves as a ClpS1 binding site.

ClpF Facilitates ClpS1 Recruitment to ClpC Chaperones

Size-exclusion chromatography (SEC) of chloroplast stromal proteome, as well as interaction assays with recombinant proteins, previously demonstrated that ClpS1 interacts with ClpC1/2 chaperones (Nishimura et al., 2013). Given the observed direct interactions between ClpF and ClpS1 described above, we examined a possible function of ClpF in this ClpS1-ClpC1/2 interaction. Stromal proteins from wild-type and *clpf-1* chloroplasts were separated by SEC and analyzed by immunoblotting for the Clp subunits (Figure 5A). In wild-type stroma, ClpS1 was present as a monomer (fractions 9 and 10) and in complexes with molecular masses ranging from 150 to 600 kD (fractions 4 to 6) (Figure 5A, upper panel). These complexes comigrated with ClpC1/2 proteins, which is consistent with the presence of ClpS1-ClpC1/2 oligomers. ClpF eluted in a mass range of ~29 to 150 kD (fractions 6 to 9), suggesting monomeric and oligomeric states. Pull-down experiments showed that recombinant GST-ClpF and ClpF-His_6 were unable to bind to each other (Figure 5B), suggesting that ClpF does not form homo-oligomeric complexes. However, because these experiments involved recombinant proteins, we cannot exclude the possibility that ClpF could make homo-oligomers in vivo. (Hetero)oligomeric ClpF coeluted with ClpC1/2 and ClpS1 in fraction 6 (~150 kD), which is compatible with an endogenous ClpS1-ClpF-ClpC1/2 complex. Strikingly, the native mass distribution of ClpS1 proteins was dramatically different in stromal proteome of *clpf-1* (Figure 5A, lower panel). In *clpf-1*, ClpS1 was predominantly in a monomeric state (fractions 9 and 10) and largely missing in the higher molecular mass range, suggesting that loss of ClpF strongly reduced the association of ClpS1 with ClpC chaperones. Consistently, the migration of ClpC proteins shifted toward lower molecular mass ranges, presumably due to the loss of ClpF and/or ClpS1 (Figure 5A). In wild-type stroma, but only at very low levels in *clpf-1* stroma, ClpS1 and ClpC1/2 were also detected in complexes between 200 and 600 kD (fractions 4 and 5) where there was no significant amount of ClpF. This indicates that ClpS1 can also interact with ClpC1/2 independent of ClpF (in agreement with previous in vitro experiments; Nishimura et al., 2013) but that ClpF enhances interactions between ClpS1 and the ClpC chaperones, with ClpF possibly recruiting ClpS1 to ClpC.

The observed oligomeric states in the wild type and *clpf-1* in the SEC experiments suggest that ClpS1 interactions with ClpC chaperones involve ClpF binding to the chaperones. To further test the ClpF interaction with ClpC1/2 and test the ClpF recruitment model of ClpS1, we performed three sets of GST pull-down experiments with recombinant full-length ClpF, ClpS1, and ClpC2 (Figures 5C to 5E). Full-length ClpF and ClpC2 proteins indeed directly interacted with high efficiency without any other requirements (Figure 5C). The lack of observation of this interaction using co-IPs with anti-ClpF antibody against the wild-type chloroplast stromal proteome (Figure 2D) suggests their association is transient in vivo. The second set (Figure 5D) showed that ClpC2 and ClpS1 coeluted with ClpF; this suggests that ClpF, ClpS1, and ClpC2 can form a complex or, alternatively, that ClpS1 and ClpC bind to different regions of ClpF in a noncompetitive manner. The ClpS1 association with the ClpC chaperones was relatively weak, but ClpF greatly stimulated this interaction (Figure 5E). Together, these findings suggest that ClpF facilitates the recruitment of ClpS1 to the ClpC chaperones through interaction of ClpF with ClpC, which is fully consistent with the results of SEC experiments using stromal proteomes.

ClpF Interacts with ClpC through Both Its NTD and uvrB/C Domains, but Not YccV

To determine the domains responsible for interaction between ClpF and ClpC1/2, we performed a ClpC and ClpF affinity experiment using different ClpF and ClpC1/2 regions (Figures 6A to 6E; summarized in Figure 6F). This showed that ClpF could bind to full-length ClpC2 through both its NTD and uvrB/C domain, but not its YccV-like domain (Figure 6B). The ClpC1/2 primary structure contains an N-domain for adaptor binding, followed by two ATPase domains (AAA1 and AAA2) for substrate translocation and unfolding (Figure 6A). The pull-down assays showed that the NTD of ClpF can interact with the N-domain of ClpC (Figure 6C). Interestingly, ClpF binding to ClpC1/2 N-domains was stimulated by ClpS1, with a stronger effect on the binding to ClpC2 than to ClpC1 (Figure 6D). Finally, the ClpF-uvrB/C domain weakly interacts with the ClpC middle region, downstream of the N-domain (Figure 6E).

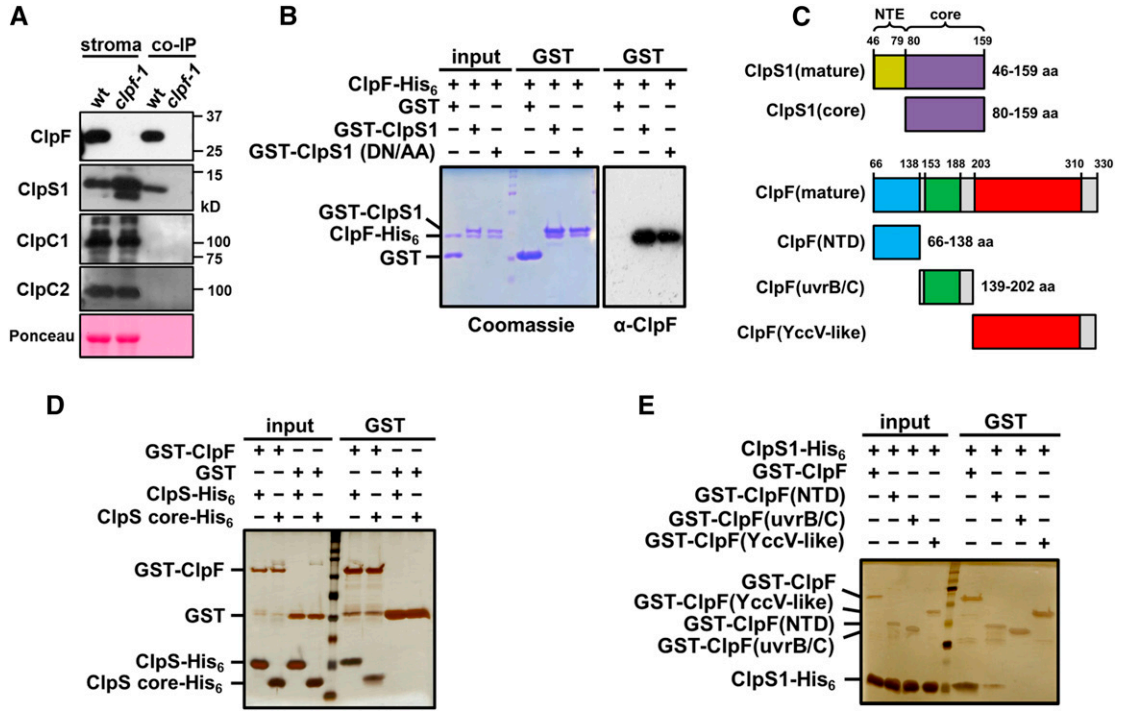

Figure 4. Mapping the Interactions between ClpF and ClpS1.

(A) Co-IP using ClpF-specific antiserum with chloroplast stromal proteome demonstrates the interaction between endogenous ClpF and ClpS1. No interactions were observed between endogenous ClpF and ClpC1,2 in this assay. Ponceau-stained blot shows Rubisco large subunit as the loading control.
(B) GST pull-down assay for ClpF interaction with the wild type and mutant (D89A/N90A) of ClpS1. Purified N-terminal GST fusions (3.6 μM GST or 2.5 μM GST-ClpS1) and C-terminal His_6-tagged ClpF (3.0 μM ClpF-His_6) were incubated at room temperature for 90 min (labeled "input" above the panel), bound to glutathione sepharose resin and eluted with Laemmli buffer (labeled "GST" above the panel), followed by SDS-PAGE and Coomassie staining. Inputs (10%) and 67% of total eluates were loaded in each lane. Similar labeling (input and GST) is used for pull-down experiments in Figures 5 to 7. The Asp-89 and Asn-90 residues are conserved across ClpS proteins and have been demonstrated to be essential for substrate binding (Nishimura et al., 2013). The right-hand panel shows the immunoblot with anti-ClpF antibody.
(C) Functional domains for ClpF and ClpS1.
(D) and **(E)** GST pull-down assays to determine which domains of ClpS1 interact with ClpF **(D)** and which domains in ClpF interact with ClpS1 **(E)**. In **(D)**, GST (3.6 μM) or GST-ClpF (1.7 μM) was combined with ClpS1-His_6 (7.5 μM) or ClpS1 core-His_6 (8.8 μM), while in **(E)**, GST fusions of full-length ClpF (2.6 μM GST-ClpF) or truncated versions of ClpF (4.1 μM GST-ClpF [NTD], 4.3 μM GST-ClpF [uvrB/C], or 3.5 μM GST-ClpF [YccV]) were combined with 11 μM ClpS1-His_6. After incubation at room temperature for 90 min, the proteins were loaded onto the glutathione sepharose resin, followed by elution with Laemmli buffer. Inputs (10% **[D]** or 5% **[E]**) and 67% **(D)** or 50% **(E)** of total eluates (GST) were analyzed by gel electrophoresis. The silver-stained gel illustrates the input and resulting pull-down profiles (GST).

Figure 6F summarizes the observed domain interactions between ClpF, ClpS1, and ClpC1,2, with ClpS1 and ClpF mutually stimulating their interactions with ClpC1,2; this is compatible with the formation of a ClpS1-ClpF-ClpC complex (see Discussion).

ClpF Directly Recognizes the in Vivo Clp Substrate GluTR

GluTR is a key enzyme in tetrapyrrole biosynthesis and was identified as a ClpS1 target (Nishimura et al., 2013; Nishimura and van Wijk, 2015). We recently confirmed this interaction in planta, and in vivo analysis suggests that the GluTR level is in part regulated by the Clp system (J. Apitz, K. Nishimura, A. Wolf, B. Hedtke, K.J. van Wijk, and B. Grimm, unpublished data). Therefore, we tested the involvement of ClpF in the degradation of GluTR. Pull-down experiments with recombinant proteins showed that ClpF directly recognized GluTR through its NTD, but not through its uvrB/C or YccV domains (Figure 7A). One possible explanation for this is that interaction between ClpF and GluTR is the first step in Clp-dependent degradation of GluTR; thus, ClpF is needed for efficient interaction of ClpS1 with substrate GluTR. Hence, in our initial observation of both GluTR and ClpF1 in ClpS1 affinity experiments with stroma (Nishimura et al., 2013), we may have captured a ClpS1-ClpF-GluTR interaction. Comparison of GluTR accumulation across the wild type, *clpf-1*, *clpf-2*, *clps1*, and the double mutant *clpf-1 clps1* showed that GluTR abundances were increased in these null alleles (Figure 7B). Combining both in vitro and in vivo data suggests that ClpF regulates GluTR abundance through its direct recognition and stimulation of the delivery of ClpS1-GluTR to the ClpC chaperones, as summarized in a conceptual, but as this point speculative model (Figure 7C, pathway 1).

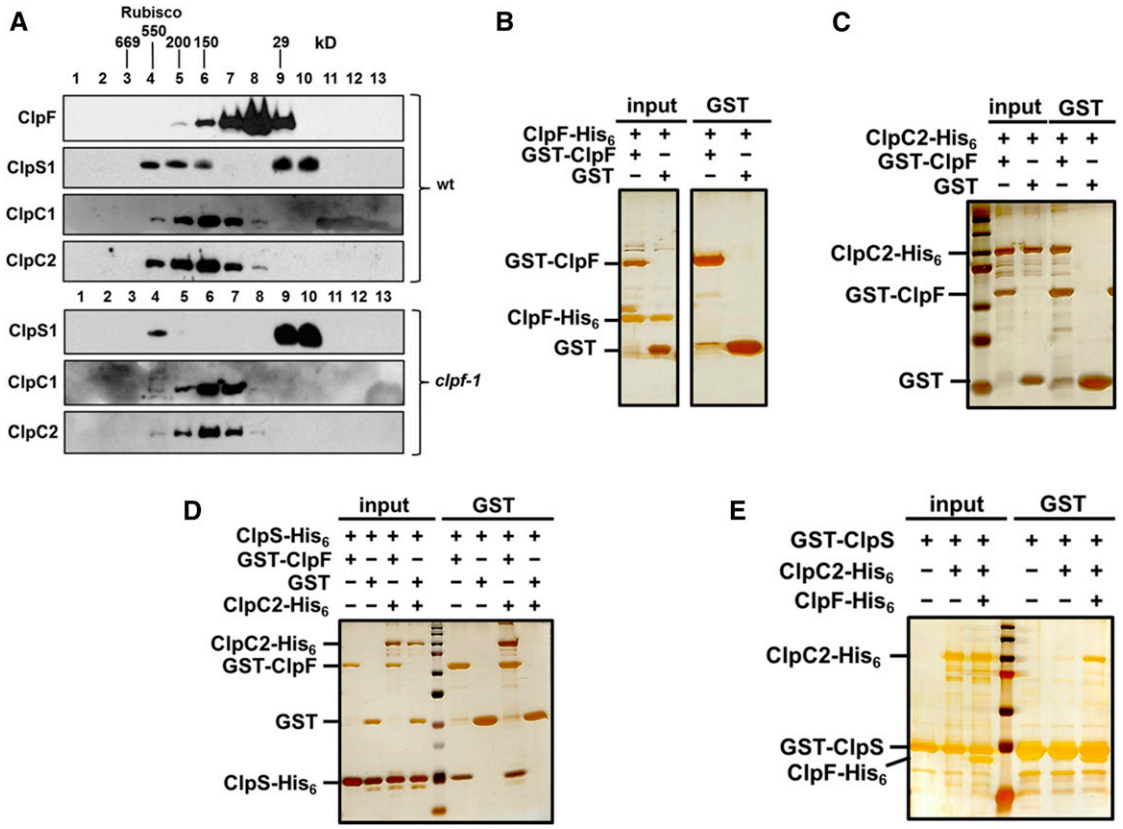

Figure 5. ClpF Facilitates ClpS1 Recruitment to the ClpC Chaperone in Vivo and in Vitro.

(A) SEC experiment of wild-type and *clpf-1* stromal proteomes. After SEC, an equal volume of each fraction (fractions 1 to 13) was separated by SDS-PAGE, followed by immunoblotting with ClpF-, ClpS1-, ClpC1-, and ClpC2-specific antibodies. The peak accumulations of native molecular markers separated by SEC under the same conditions are indicated.

(B) GST pull-down analysis for ClpF interaction with itself. Purified GST alone (7.1 μM) or GST-fused ClpF (3.4 μM GST-ClpF) and His_6-tagged ClpF (6.1 μM ClpF-His_6) were incubated at room temperature for 60 min (input), bound to glutathione sepharose resin, and eluted with Laemmli buffer (GST), followed by SDS-PAGE and silver staining. Inputs (5%) or 50% of total eluates (GST) were loaded in each lane.

(C) Pull-down assay for ClpF interaction with full-length ClpC2 chaperone. GST alone (4.8 μM) or GST-fused ClpF (2.3 μM GST-ClpF) and ClpC2-His_6 (1.3 μM) were incubated at room temperature for 90 min, combined with the glutathione sepharose resin and eluted with Laemmli buffer. Inputs (5%) and 50% of the eluates (GST) were analyzed by SDS-PAGE and silver nitrate staining.

(D) Pull-down assays showing that ClpC2 copurifies with a binary complex comprising ClpS1 and ClpF. GST (7.1 μM) or GST-ClpF (3.4 μM) and ClpS1-His_6 (15 μM) were incubated at room temperature for 90 min with or without ClpC2-His_6 (2.0 μM). The proteins were bound to the glutathione sepharose resin and eluted with Laemmli buffer, followed by SDS-PAGE and silver nitrate staining. Each lane contains 5% of inputs or 50% of total eluates (GST).

(E) Pull-down assays showing that ClpF enhances ClpS1 interaction with the ClpC chaperone. GST-ClpS1 (5.8 μM) was incubated at room temperature for 90 min with ClpC2-His_6 (2.3 μM) in the presence/absence of ClpF-His_6 (7.0 μM). The mixture was combined with the glutathione sepharose resin, followed by elution of the proteins with Laemmli buffer. Inputs (3.8%) and 50% of the eluates (GST) were subjected to SDS-PAGE and silver nitrate staining.

DISCUSSION

ClpF: A Novel Clp Protease Adaptor with a Unique Tripartite Domain Structure

The Clp system is found in nonphotosynthetic and photosynthetic prokaryotes and in mitochondria and/or plastids in all studied eukaryotes (Sauer and Baker, 2011; Battesti and Gottesman, 2013; Liu et al., 2014; Nishimura and van Wijk, 2015). Throughout evolution, a highly interesting diversification of Clp chaperones, protease core composition, and oligomeric state, as well as adaptors and antiadaptors has occurred, in part to accommodate the vast range of (sub)cellular proteomes, life cycles, and environments. Clp adaptors modulate the substrate selection of the Clp protease, typically by first binding to the substrate(s) and then delivering it to the ATP-dependent Clp chaperone (Kirstein et al., 2009). The binding of the adaptor to the chaperone N-domain can also by itself change the affinity of the chaperone for different substrate classes (Kirstein et al., 2009; Battesti and Gottesman, 2013). Various Clp adaptors have evolved for bacterial ClpXP, ClpAP, and ClpCP chaperone-protease systems. Adaptors recognize a specific tag, such as *E. coli* SspB recognizing the SsrA tag or ClpS recognizing N-degrons. Alternatively, Clp adaptors recognize a specific protein, such as cyanobacterial NblA targeting

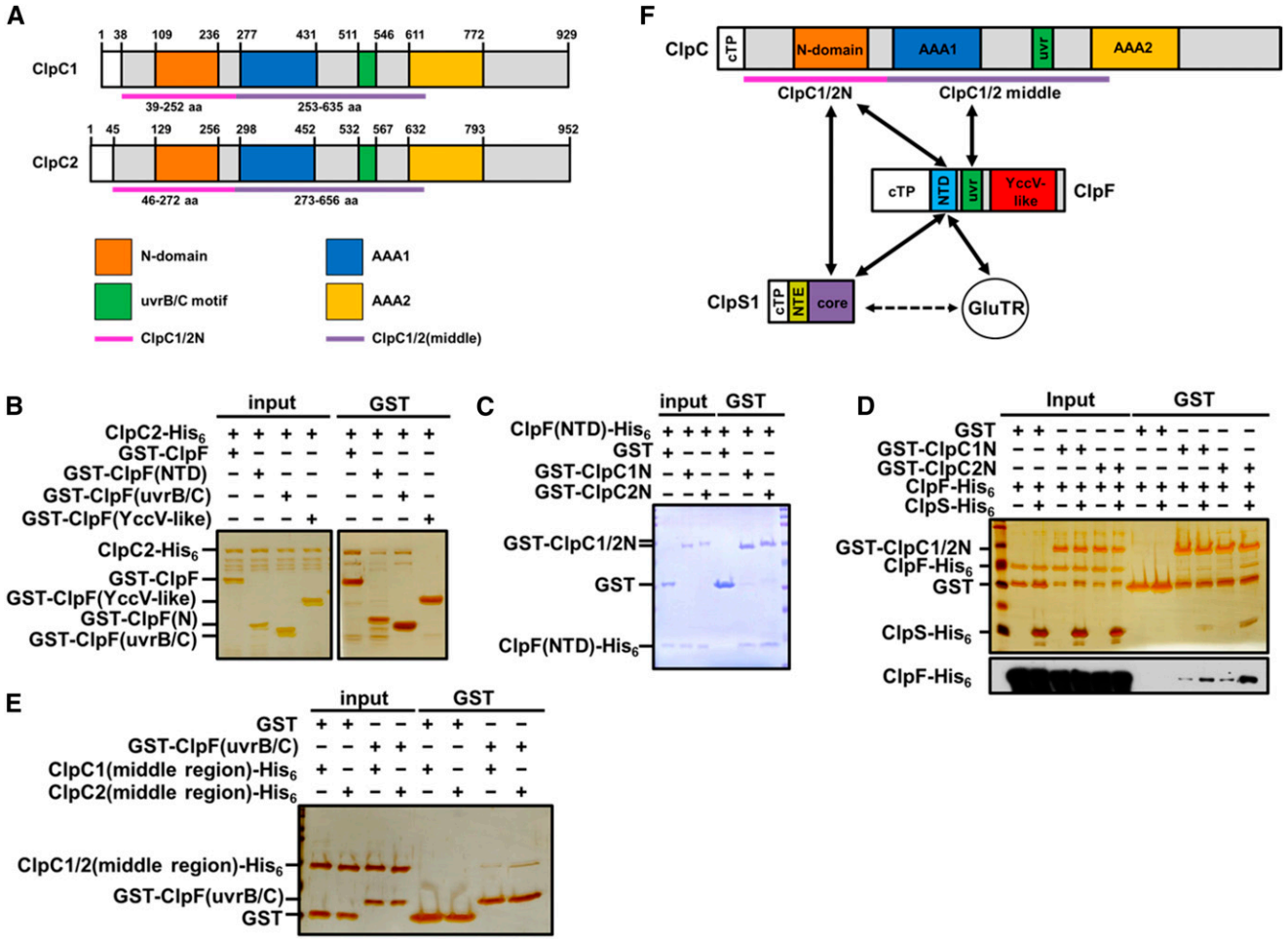

Figure 6. Mapping the Interactions between ClpF and the ClpC Chaperones.

(A) Illustration of the ClpC1/2 primary structures. ClpC1 and ClpC2 comprise an N-domain (orange) for adaptor and substrate binding, two ATPase domains (AAA1,2; blue and yellow) for substrate unfolding and translocation to the core, and uvrB/C motif (green) of unknown function.

(B) GST pull-down assays showing that ClpF interacts with ClpC through its NTD and uvrB/C, but not though the YccV domain. GST fusions of full-length ClpF (2.6 μM GST-ClpF) or three separate domains of ClpF (4.1 μM GST-ClpF [NTD], 4.3 μM GST-ClpF [uvrB/C], or 3.5 μM GST-ClpF [YccV]) were incubated for 90 min at room temperature with ClpC2-His_6 (1.5 μM), followed by binding to the glutathione sepharose resin and elution with Laemmli buffer. Inputs (5%) and 50% of the eluted proteins were separated by SDS-PAGE and visualized by silver staining.

(C) Pull-down assays showing that ClpF NTD interacts with the ClpC1/2 N-domains. GST alone (2.7 μM) or GST-fused N-domain of ClpC1/2 (1.5 μM GST-ClpC1N or 1.4 μM GST-ClpC2N) was incubated at room temperature for 120 min with His_6-tagged N-terminal domain of ClpF (8.9 μM ClpF[NTD]-His_6). The protein mixture was subjected to binding to the glutathione sepharose resin, followed by elution with Laemmli buffer. Inputs (5%) and 70% of the protein eluates were analyzed by SDS-PAGE and Coomassie staining.

(D) Pull-down assays showing that interactions between ClpF and the ClpC1/2 N-domains are stimulated by ClpS1. GST alone (2.7 μM) or GST-fused N-domain of ClpC1/2 (1.4 μM GST-ClpC1/2N) and ClpF-His_6 (3.0 μM) were incubated at room temperature for 90 min in the presence/absence of ClpS1-His_6 (7.5 μM), followed by binding to the glutathione sepharose resin and elution with Laemmli buffer. The proteins were separated by SDS-PAGE and visualized with silver nitrate and by immunoblots also for ClpF-His_6. Each lane contains 5% of inputs or 70% of total eluates (GST).

(E) Pull-down assays showing that the ClpF uvrB/C motif interacts with a segment downstream of the ClpC N-domains (middle region). GST alone (2.7 μM) or GST-fused uvrB/C motif of ClpF (2.2 μM GST-ClpF[uvrB/C]) and His-tagged middle region of ClpC1/2 (2.2 μM ClpC1/2 [middle region]-His_6) were incubated for 90 min at room temperature. The proteins were bound to the glutathione sepharose resin and then eluted with Laemmli buffer, followed by SDS-PAGE and silver staining. Inputs (5%) or 70% of total eluates (GST) was loaded in each lane.

(F) Summary of the observed domain interactions between ClpF, ClpS1, and ClpC1,2 as indicated by solid lines with arrows, with ClpS1 and ClpF mutually stimulating their interactions with ClpC1,2; this is compatible with a ClpS1-ClpF-ClpC complex. The dashed line indicates the in vitro interaction observed previously using ClpS1 affinity columns and isolated stromal proteomes (Nishimura et al., 2013).

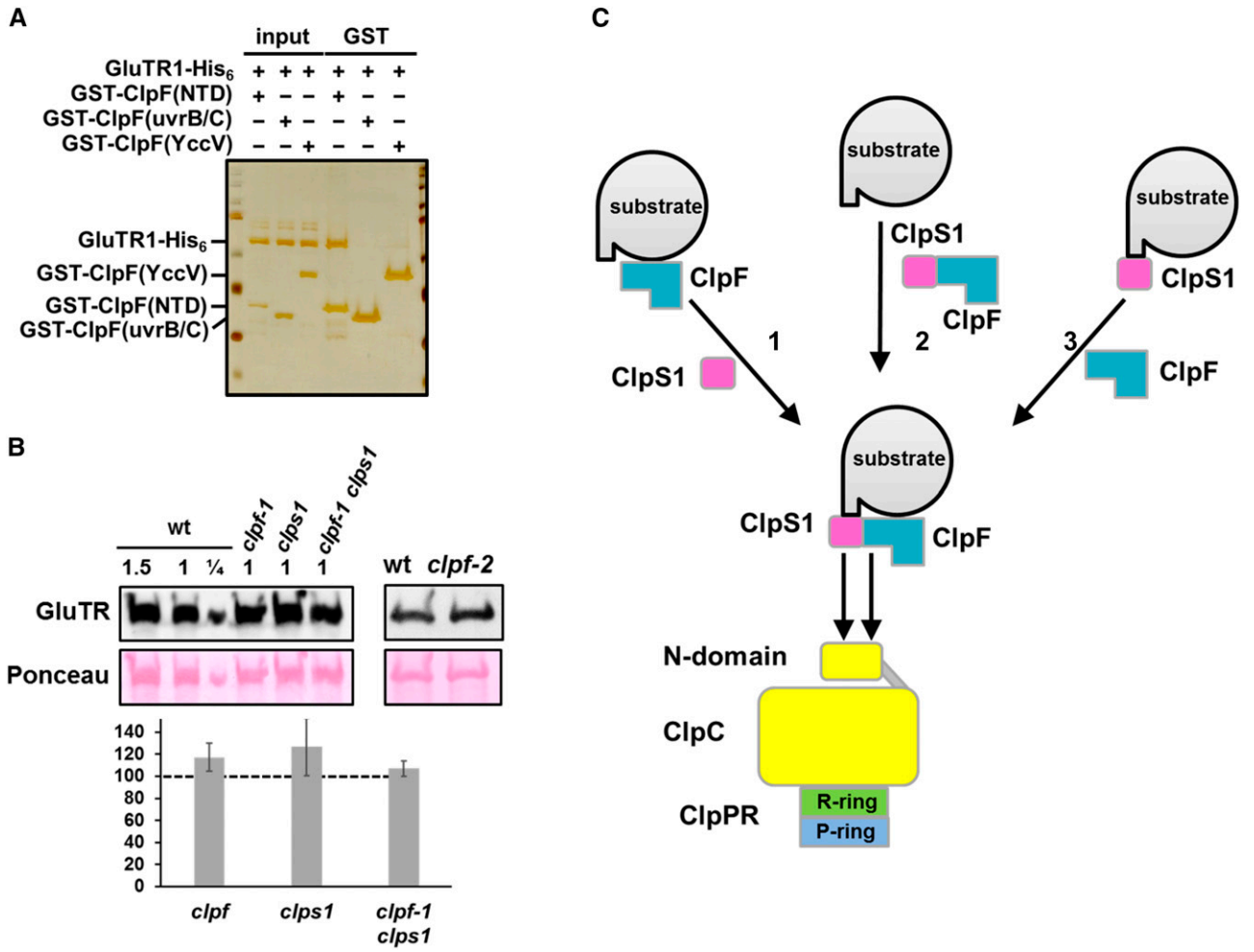

Figure 7. ClpF Recognizes and Delivers the in Vivo Substrate, GluTR, to the ClpC1/2 Chaperones in Collaboration with ClpS1.

(A) Pull-down assays showing that ClpF NTD (left-hand panel) directly recognizes the in vivo substrate GluTR. GST fusions of truncated versions of ClpF (2.1 μM GST-ClpF [NTD], 2.2 μM GST-ClpF [uvrB/C], or 1.7 μM GST-ClpF [YccV]) and GluTR1-His_6 (1.8 μM) were incubated for 90 min at room temperature. The mixture was combined with the glutathione sepharose resin, and the proteins were eluted with Laemmli buffer and analyzed by SDS-PAGE and silver nitrate staining. Each lane contains 5% of inputs or 70% of the eluates.

(B) Increased accumulation of GluTR in *clpf* and *clps1* mutants. Total leaf extracts from wild-type and *clpf* mutant alleles (25 μg [1×] or the indicated dilutions in left panel; 15 μg for each lane in right panel) were analyzed by immunoblotting with anti-GluTR antibody. Seedlings were grown under short- or long-day light conditions for ~15 d on agar plates (see Methods) and harvested in developmental stage 1.06-1.07. The bar diagram shows quantification of GluTR immunoblot signal across multiple independent experiments (the standard deviations are indicated) with the $n = 8$ (*clpf* alleles), 6 (*clps1*), or 3 (*clpf clps1*). The *y* axis of the bar diagram shows relative GluTR abundance compared to the wild type (in %). GluTR levels were significantly increased ($P < 0.05$; Student's *t* test) in *clpf*.

(C) Conceptual models for substrate recognition and delivery to the ClpC chaperone by the combined action of ClpS1 and ClpF. The model shows three pathways for delivery of substrate to ClpC. In pathway 1, ClpF binds to the substrate, followed by a ClpS stimulated binding of this ClpF substrate complex to ClpC. In pathway 2, a ClpS1-ClpF complex recognized and binds the substrate, after which the ClpS1-ClpF substrate complex binds to ClpC. In pathway 3, ClpS1 binds to the substrate, followed by a ClpF-stimulated binding of this ClpS1 substrate complex to ClpC. Each of the three models seems compatible with the experimental data, but we favor pathways 1 or 2, based on our observations.

phycobilosomes (Baier et al., 2014) or *E. coli* adaptor RssB specifically delivering sigma factor RpoS to ClpXP (Battesti and Gottesman, 2013). In addition to our proposed ClpS1-ClpF multiprotein adaptor in chloroplasts (Figure 7C), one other multiadaptor has been described so far. This multiadaptor system, which is found in the α-proteobacterium *Caulobacter crescentus* and consists of the proteins CpdR, PopA, and RcdA, delivers a transcriptional regulator (CtrA) to ClpXP for degradation (Smith et al., 2014). This multiprotein adaptor system appears to be highly specific for CtrA, e.g., as suggested by direct transcriptional regulation of RcdA by CtrA and a shared phosphotransferase between CtrA and CpdR, and is essential for degradation when CtrA is bound to DNA. This multiprotein adaptor system is not essential for in vitro CtrA degradation by ClpXP but does

accelerate CtrA degradation 10-fold without changing the V_{max}, which is consistent with a "classical" adaptor (Smith et al., 2014). Our discovery of a multimeric adaptor system for plastid Clp machinery suggests that there may be a complex regulatory mechanism for substrate recognition and delivery in chloroplasts.

The only Clp adaptors known in eukaryotes are the ClpS homologs in plastids (Nishimura and van Wijk, 2015). No adaptor is known for the mitochondrial ClpXP systems in animals or plants. In this study, we firmly establish (1) ClpF as a functional partner of ClpS1 through in vitro and in vivo interaction assays, and unlike several other ClpS1 interactors (likely representing protease substrates), ClpF interaction does not depend on the conserved ClpS1 substrate binding residues; (2) that ClpF interacts with ClpC1,2 chaperones and recognizes the in vivo substrate GluTR; and (3) that ClpF and ClpS1 mutually stimulate their interactions with ClpC through at least three possible pathways (Figure 7C). Based on these experimental data, we propose a noncanonical pathway of Clp substrate recognition and delivery involving a binary adaptor system consisting of ClpF-ClpS1. Phylogenetic analysis showed that ClpF is unique to photosynthetic eukaryotes but is confined to plastids. Hence, ClpF represents an evolutionary adaptation of the plastid Clp system.

ClpF and ClpS1 Play Partially Overlapping Roles in Plastid Proteome Homeostasis

Comparative proteomics analysis of the *clpf-1* mutant showed that the chloroplast stromal proteins ClpB3 and HSP90 were significantly downregulated. ClpB3 is the functional homolog of bacterial ClpB, and its role is to help unfold proteins that are either aggregated or otherwise misfolded (Myouga et al., 2006; Lee et al., 2007; Carroni et al., 2014), whereas HSP90 is generally involved in late stages of protein folding and holoenzyme formation (Wandinger et al., 2008). This downregulation strongly contrasts with the chaperone response in loss-of-function mutants for ClpC1, ClpT1,2, and ClpPR core proteins; all of these mutants show a pronounced 5- to 10-fold increase in ClpB3 levels, as well as significant increases in the levels of other stromal chaperones, including CPN60, HSP70, and HSP90 homologs (Nishimura and van Wijk, 2015). Furthermore, we showed that the double mutant of *clpr2-1* (a leaky allele in *CLPR2*) and the *CLPB3* null mutant are seedling lethal (Zybailov et al., 2009). This strongly suggests that the Clp chaperone and protease capacity is needed for general protein homeostasis and removal of protein aggregates or that loss of Clp protease capacity results in protein aggregation. Downregulation of the Clp core protease capacity in the green alga *Chlamydomonas reinhardtii* also resulted in upregulation of chloroplast chaperone system in addition to many other pleiotropic effects (Ramundo et al., 2014). In contrast, and assuming that high ClpB3 levels reflect the accumulation of aggregates, neither ClpF nor ClpS1 appears to play a role in selection and degradation of chloroplast protein aggregates nor does loss of their function induce such pronounced unfolding response (Dougan et al., 2002). Interestingly cyanobacterial ClpC shows an intrinsic disaggregation ability independent of ClpS proteins (Andersson et al., 2006). Furthermore, plastid ClpC by itself also displays some ability for in vitro disaggregating/folding activity (Rosano et al., 2011).

The completely opposite accumulation patterns of HDS, a central enzyme in the MEP pathway, between the null mutants for the two adaptors (ClpS1 and ClpF) and null or knockdown mutants for the rest of the Clp system (chaperones and protease core) is intriguing. Whereas HDS levels were reduced in *clpf-1* and *clps1*, they were 2- to 10-fold increased in Clp mutants with limited chaperone or protease capacity (Kim et al., 2015; Nishimura and van Wijk, 2015). The substrate for HDS is MEcPP, a demonstrated signaling molecule that functions as a stress signal modifying nuclear gene expression (Xiao et al., 2012; Grimm et al., 2014), and HDS activity must therefore be carefully regulated. We did identify HDS as a ClpS1 target in the GST-ClpS1 affinity experiments using stroma of *clps1 clpc1* with upregulated HDS levels (Nishimura et al., 2013). Considering all data, HDS is likely degraded by the Clp system, but multiple factors regulate its protein level and activity. It was noted that HDS, together with HDR immediately downstream of HDS, constitutes the light-regulated portion of the MEP pathway (Banerjee and Sharkey, 2014). Future studies should investigate the posttranslational mechanisms governing the stability of this candidate Clp target.

A ClpF-ClpS1 Multisubunit Adapter Model in Chloroplasts

Figure 7C shows conceptual, testable models for substrate delivery to the ClpC chaperones, incorporating the observed interaction between ClpF and ClpS1 (Figure 4), the dramatic shift in oligomeric state of ClpS1 as observed by SEC in *clpf-1* stroma compared with the wild type (Figure 5A), the observed mutual stimulatory effect of ClpF on ClpS1 association with ClpC chaperones (Figures 5A, 5E, and 6D), the in vitro interactions between ClpF and ClpC1 and ClpC2 (Figure 6), and the in vitro observations of substrate GluTR interaction with ClpF (Figure 7A). The model proposes that ClpF, ClpS1, or a ClpF-ClpS1 complex recognizes substrates in the stroma, thus forming a ClpF-ClpS1 adaptor complex with the substrate. This ClpF-ClpS1 substrate complex then binds to ClpC1/2, in particular driven by ClpF-ClpC interactions, but with ClpF and ClpS1 also mutually stabilizing their binding to the chaperone. The proposed model represents a novel type of substrate delivery mechanism that is unique to ClpS1; this model now needs to be rigorously tested, and specific ternary and possible quaternary interactions (between ClpF, ClpS1, ClpC, and substrate GluTR1), further mechanistic details, and participation in delivery of substrates other than GluTR1 remain to be determined. Details regarding GluTR1 as substrate for recognition and degradation by Clp need to be addressed. In this context, it is important to note that GluTR1 in vivo forms a V-shaped dimer that is proposed to interact with glutamate 1-semialdehyde aminotransferase, the enzyme immediately downstream of GluTR, allowing for efficient channeling of substrates (Sauer and Camper, 2001; Moser et al., 2002; Zhao et al., 2014). GluTR1 is under various types of posttranslational regulatory mechanisms, involving the GluTR binding protein (Czarnecki et al., 2011; Zhang et al., 2015) and the negative regulator Flu in darkness (Kauss et al., 2012), as well as metabolic regulation by heme (reviewed in Czarnecki and Grimm, 2012). The conditions for in vivo recognition of GluTR by ClpF and ClpS1 remain to be determined and will likely involve competition between GluTR interactors and GluTR structural changes. Interestingly,

proteolysis of GluTR in the gram-negative bacterium *Salmonella typhimurium* is also regulated by the ClpAP system as well as LON protease and requires the N-terminal region of GluTR (Wang et al., 1999a, 1999b).

Possible Downstream Events of Substrate Delivery: Fine-Tuning of ClpS1 Activity

We observed >3-fold ClpS1 overaccumulation in *clpf-1*, which was not due to enhanced *CLPS1* mRNA levels, but either due to increased translation or increased stability. Interestingly, the cyanobacterial adaptor protein NblA, which recognizes and delivers phycobilisomes to the Clp chaperone for degradation, is degraded together with its substrates by Clp (Baier et al., 2014). Also, the *Bacillus subtilus* Clp adaptor MecA, and its anti-adaptor ComS, are degraded by the Clp system (Battesti and Gottesman, 2013). Based on our model that ClpF recruits ClpS1 to the ClpC chaperones for substrate delivery, ClpS1 overaccumulation could then be explained by hypothesizing that ClpS1 is degraded together with its substrate by the Clp system. In *clpf-1*, where ClpS1 recruitment to the chaperone is inefficient, ClpS1 would become stabilized due to its delayed substrate delivery. Consistently, ClpS1 levels also increased in the *clpc1* null mutant (Nishimura et al., 2013). The constitutive accumulation of ClpF throughout the life cycle of the leaf (and chloroplast) but the developmentally regulated accumulation of ClpS1 (high in young leaves and low in old leaves) is consistent with a more specific, fine-tuning role of ClpS1. The identification of GluTR as a substrate of ClpS1 is also consistent with such a role because GluTR is most important in developing tissue. The possible degradation of chloroplast ClpS1 by the Clp system warrants further investigation, in particular since it would provide an elegant mechanism to further fine-tune proteolysis in plastids. So far, there is no other evidence for other multiprotein adaptor systems for Clp proteases, but it is quite possible that they exist for other ClpS homologs or other adaptors.

METHODS

Plant Material, Mutant Isolation, and Growth Conditions

Arabidopsis thaliana T-DNA insertion lines SALK_014112C (for *clpf-1*) and GK-229G07 (for *clpf-2*) were obtained from the Arabidopsis Biological Resource Center. Genomic PCR were performed as before (Nishimura et al., 2013). For RT-PCR, total RNA was isolated with an RNeasy plant mini kit (Qiagen). The first strand was synthesized from equal amounts of total RNA with Superscript III Reverse Transcriptase (Invitrogen). Primers used for genotyping and RT-PCR are listed in Supplemental Data Set 4. The positions of the T-DNA insertions were confirmed by DNA sequencing. The *clps1* null mutant was described previously (Nishimura et al., 2013). Wild-type and mutant plants were grown on soil or Murashige and Skoog plates (0.5× strength Murashige and Skoog salts [Sigma-Aldrich], 1× vitamin mixture [Sigma-Aldrich], 2% sucrose, and 0.6% Phytoblend [Caisson Laboratories], pH 5.7) in a growth chamber under long or short day/night cycles at 100 μmol photons m^{-2} s^{-1}, 23°C/darkness (21°C).

Phylogenetic Analysis and Structure Prediction

The 34 ClpF protein sequences were collected from Phytozome v9 (http://www.phytozome.net/) and were aligned using MUSCLE (http://toolkit.tuebingen.mpg.de/muscle) with 30 iterations and ClustalW output format. The aligned sequences were edited to remove gaps, insertions, and extensions with Jalview (http://www.jalview.org/), and the sequence alignment was then converted to the PHYLIP format. A phylogenetic inference was generated using RAxML HPC BlackBox interface with the general time reversal model of the protein substitution matrix on the CIPRES Science Gateway (http://www.phylo.org/index.php/portal/). The resulting phylogenetic tree was obtained by FigTree (http://tree.bio.ed.ac.uk/software/figtree/), and significant RAxML bootstrap support values (>50) were indicated at the nodes of the tree. The multiple sequence alignment is available in Supplemental File 1. A ClpF three-dimensional structure was predicted with the mature sequence (amino acids 66 to 330) using I-TASSER (http://zhanglab.ccmb.med.umich.edu/I-TASSER/) (Yang et al., 2015).

DNA Construction, Protein Expression, and Purification

The gene products for full-length and partial sequences of ClpS1, ClpF, ClpC1, and ClpC2 were amplified using Arabidopsis cDNA as a template with the specific primer pairs and directly introduced into the expression vectors after restriction enzyme treatment. Primer sequences are listed in Supplemental Data Set 4. The plasmids expressing His-tagged ClpS1, ClpF, and ClpC2, and GST-fused ClpS1 and ClpC1N were described previously (Nishimura et al., 2013). Protein expression was induced in Rosetta (DE3) strain (Novagen) at 28°C (for ClpC2-His and GST-ClpC2N) or 37°C (for the others) for 3 h with 0.5 or 1 mM isopropyl-1-thio-β-D-galactopyranoside. GST and GST fusion proteins were extracted in a buffer containing 40 mM Tris-HCl (pH 7.5), 5 mM EDTA, and 0.5% Triton X-100 and purified with Glutathione Sepharose 4B (GE Healthcare Life Sciences) and 10 mM reduced glutathione (Sigma-Aldrich) in the extraction buffer. His-tagged proteins were extracted and purified through Ni-NTA agarose (Qiagen). Purified proteins were buffer exchanged to TBS buffer through PD MiniTrap G-25 column (GE Healthcare Life Sciences), combined with glycerol to 50% (final concentration), and stored at −20°C until use. Protein concentrations were determined using the Bradford protein assay (Bio-Rad) with BSA as the standard.

GST Pull-Down Assay

GST or GST fusion proteins were incubated with His-tagged proteins in 100 to 150 μL of a mixture containing 20 mM Tris-HCl, pH 7.5, 100 mM NaCl, and 15 to 25% glycerol under the conditions as indicated in the legends for each experiments. After removing 10% of each sample as the input sample, the mixture was further incubated at 4°C for 30 min with Glutathione Sepharose 4B (GE Healthcare Life Science; 20 μL of the resin slurry). Protein-bound resin was washed five times with 10 column volumes of the buffer (25 mM Tris-HCl, pH 7.5, 2 mM EDTA, 100 mM NaCl, and 0.5% Triton X-100). Proteins were eluted with 1.5 column volumes of 3× Laemmli buffer minus β-mercaptoethanol by heat treatment at 75°C for 5 min and analyzed by SDS-PAGE and silver nitrate or Coomassie Brilliant Blue staining.

Chloroplast Isolation, Stromal Protein Preparation, and Total Leaf Protein Extraction

Chloroplasts were isolated at leaf stage 1.06 to 1.08 and separated into stromal and membrane fractions essentially as described by Olinares et al. (2010). Total leaf proteins were extracted as described earlier (Friso et al., 2011).

Coimmunoprecipitations

Co-IP experiments were performed essentially as described previously (Asakura et al., 2012), using ClpF antibody generated previously (1:7500; see Nishimura et al., 2013), co-IP buffer (20 mM Tris-HCl, pH 7.5, 100 mM

NaCl, 1 mM EDTA, 15% glycerol, 0.1% Igepal CA-630, and 5 μg mL^{-1} aprotinin), and 200 μg of stromal fractions isolated from wild-type and *clpf-1* mutant chloroplasts.

Size-Exclusion Experiments

Chloroplast stroma was fractionated on a size-exclusion column as described (Olinares et al., 2010). Stromal proteins (0.16 to 0.19 mg) were eluted in a buffer containing 25 mM HEPES, pH 8.0, 10 mM NaCl, and 10 mM $MgCl_2$. Subfractions were combined as follows: six for fractions 1 to 3, four for fractions 4, three for fractions 5 to 11, and six for fraction 12 and 13. Proteins in combined fractions were precipitated with trichloroacetic acid/acetone and solubilized with 30 μL of 3× Laemmli buffer followed by SDS-PAGE and immunoblot analyses.

Immunoblot Analysis

Stromal proteins or total leaf extracts were separated on 12 to 15% Laemmli gels, electroblotted onto polyvinylidene fluoride membranes, and probed with specific antibodies using chemiluminescence for detection following standard procedures. The antisera raised against Arabidopsis ClpC1 and ClpC2 subunits (each at 1:4000 dilution) were kindly provided by Steven Rodermel. The antisera against Arabidopsis ClpF (previously named UVR), ClpS1, ClpP6, and ClpR2 were described previously and were used at dilutions of 1:7500, 1:1500, 1:2000, and 1:10,000, respectively (Asakura et al., 2012; Kim et al., 2013; Nishimura et al., 2013). Anti-GluTR antibody (1:5000) was from Agrisera (Sweden; Item No. AS10 689).

Comparative Proteomics of Stromal Proteomes

Stromal proteins were separated (40 μg/lane) on 10.5 to 14% precast polyacrylamide gel (Bio-Rad), followed by staining with Coomassie Brilliant Blue R 250. Each of the nine gel lanes were cut into 11 bands followed by reduction, alkylation, and in-gel digestion with trypsin as described (Shevchenko et al., 2006; Friso et al., 2011). The resuspended peptide extracts were analyzed by data-dependent MS/MS using an on-line LC-LTQ-Orbitrap (Thermo Electron) as described (Kim et al., 2015). Mass spectrometry data processing, data searching against TAIR10 using Mascot, and subsequent filtering and quantification based on normalized and adjusted spectral counts was performed as described (Nishimura et al., 2013). For our functional analyses, we only considered confirmed stromal proteins (Supplemental Data Set 2B). Pairwise significance analyses for genotypic differences was performed based on the combined outcome of two statistical packages, QSPEC and GLEE, specifically developed for spectral counting analysis, as described (Kim et al., 2015). Proteins were deemed significantly different between genotypes at $P < 0.01$ using GLEE (using NadjSPC) and with <5% false discovery rate using QSPEC (using AdjSPC).

Accession Numbers

Sequence data from this article can be found in the GenBank/EMBL libraries under the following accession numbers: UVR (ClpF), AT2G03390; ClpS1, AT1G68660; ClpC1, AT5G50920; ClpC2, AT3G48870; and GluTR, AT1G58290. Full ClpF protein sequences used for phylogenetic analysis obtained from the Arabidopsis Genome Initiative or Phytozome databases are under the following accession numbers: for Ath, AT2G03390; Ppa, Pp1s136_9V6.1; Sit, Si002169m; Sbi, Sb03g035470.1; Zma, GRMZM2G124321_T05; Bdi, Bradi2g50810.2; Osa1, LOC_Os01g55880.1; Osa2, LOC_Os08g07540.1; Mgu, mgv1a009546m; Csa, Cucsa.327730.1; Stu, PGSC0003DMP400049260; Sly, Solyc05g012620.2.1; Lus, Lus10037120; Egr, Eucgr.G02464.1; Mtr, Medtr5g043480.1; Gma1, Glyma01g06700.2; Gma2, Glyma02g12650.4; Pvu, Phvul.002G069400.1; Bra, Bra024776; Esa, Thhalv10004578m; Cru, Carubv10017613m; Aly, 904615; Aco, Aquca_002_00755.1; Vvi, GSVIVT01012177001; Gra, Gorai.013G091200.1; Tca, Thecc1EG011602t2; Csi, orange1.1g019893m; Ccl, Ciclev10032054m; Ptr, Potri.010G161600.1; Rco, 30,174.m009149; Mes, cassava4.1_011439m; Csu, 54839; Vca, Vocar20000321m; and Cre, Cre02.g113700.t1.2. Mass spectrometry-derived information, as well as annotation of protein name, location, and function for the identified proteins can be found in the PPDB (http://ppdb.tc.cornell.edu/). The mass spectrometry proteomics data have been deposited to the ProteomeXchange Consortium (Vizcaíno et al., 2014) via the PRIDE partner repository (http://www.ebi.ac.uk/pride) with the data set identifiers PXD002186 and 10.6019/PXD002186 (reviewer account details: user name, reviewer25803@ebi.ac.uk; password, wlW2QCCc).

Supplemental Data

Supplemental Data Set 1. Chlorophyll and carotenoid accumulation in wild-type, *clps1*, *clpf-1*, and *clpf-1 clps1* mutants of soil-grown plants at developmental stage 1.07.

Supplemental Data Set 2. Comparative proteomics analysis of the wild type, *clps1*, and *clpf-1*.

Supplemental Data Set 3. Chloroplast stromal proteins significantly affected in *clpf-1* or *clps1* compared with the wild type.

Supplemental Data Set 4. Primers used for genotyping, RT-PCR, and generation of recombinant proteins.

Supplemental File 1. Alignment used for phylogenetic analysis in Figure 2B.

ACKNOWLEDGMENTS

This research was supported by a grant from the National Science Foundation (MCB1021963 to K.J.v.W.) and a grant from the German Research Foundation (Deutsche Forschungsgemeinschaft, GR936 15-1 to B.G.).

AUTHOR CONTRIBUTIONS

K.N., G.F., J.A., and J.K. designed and performed the experimental analysis. L.P. carried out the statistical and correlation analyses. G.F. carried out all mass spectrometry analyses. J.A. and B.G. carried out a BiFC analysis (not included in the final version) and provided information regarding GluTR. J.K. carried out pigment analysis and growth tests. K.J.v.W. and K.N. wrote the article.

Received June 26, 2015; revised September 4, 2015; accepted September 15, 2015; published September 29, 2015.

REFERENCES

Alexopoulos, J.A., Guarné, A., and Ortega, J. (2012). ClpP: a structurally dynamic protease regulated by AAA+ proteins. J. Struct. Biol. **179:** 202–210.

Andersson, F.I., Blakytny, R., Kirstein, J., Turgay, K., Bukau, B., Mogk, A., and Clarke, A.K. (2006). Cyanobacterial ClpC/HSP100 protein displays intrinsic chaperone activity. J. Biol. Chem. **281:** 5468–5475.

Asakura, Y., Galarneau, E., Watkins, K.P., Barkan, A., and van Wijk, K.J. (2012). Chloroplast RH3 DEAD box RNA helicases in maize and Arabidopsis function in splicing of specific group II introns and affect chloroplast ribosome biogenesis. Plant Physiol. **159:** 961–974.

Baier, A., Winkler, W., Korte, T., Lockau, W., and Karradt, A. (2014). Degradation of phycobilisomes in Synechocystis sp. PCC6803: evidence for essential formation of an NblA1/NblA2 heterodimer and its codegradation by A Clp protease complex. J. Biol. Chem. **289:** 11755–11766.

Banerjee, A., and Sharkey, T.D. (2014). Methylerythritol 4-phosphate (MEP) pathway metabolic regulation. Nat. Prod. Rep. **31:** 1043–1055.

Battesti, A., and Gottesman, S. (2013). Roles of adaptor proteins in regulation of bacterial proteolysis. Curr. Opin. Microbiol. **16:** 140–147.

Carroni, M., Kummer, E., Oguchi, Y., Wendler, P., Clare, D.K., Sinning, I., Kopp, J., Mogk, A., Bukau, B., and Saibil, H.R. (2014). Head-to-tail interactions of the coiled-coil domains regulate ClpB activity and cooperation with Hsp70 in protein disaggregation. eLife **3:** e02481.

Czarnecki, O., and Grimm, B. (2012). Post-translational control of tetrapyrrole biosynthesis in plants, algae, and cyanobacteria. J. Exp. Bot. **63:** 1675–1687.

Czarnecki, O., Hedtke, B., Melzer, M., Rothbart, M., Richter, A., Schröter, Y., Pfannschmidt, T., and Grimm, B. (2011). An Arabidopsis GluTR binding protein mediates spatial separation of 5-aminolevulinic acid synthesis in chloroplasts. Plant Cell **23:** 4476–4491.

d'Alençon, E., Taghbalout, A., Bristow, C., Kern, R., Aflalo, R., and Kohiyama, M. (2003). Isolation of a new hemimethylated DNA binding protein which regulates dnaA gene expression. J. Bacteriol. **185:** 2967–2971.

Dougan, D.A., Micevski, D., and Truscott, K.N. (2012). The N-end rule pathway: from recognition by N-recognins, to destruction by AAA+proteases. Biochim. Biophys. Acta **1823:** 83–91.

Dougan, D.A., Reid, B.G., Horwich, A.L., and Bukau, B. (2002). ClpS, a substrate modulator of the ClpAP machine. Mol. Cell **9:** 673–683.

Erbse, A., Schmidt, R., Bornemann, T., Schneider-Mergener, J., Mogk, A., Zahn, R., Dougan, D.A., and Bukau, B. (2006). ClpS is an essential component of the N-end rule pathway in *Escherichia coli*. Nature **439:** 753–756.

Friso, G., Olinares, P.D.B., and van Wijk, K.J. (2011). The workflow for quantitative proteome analysis of chloroplast development and differentiation, chloroplast mutants, and protein interactions by spectral counting. In Chloroplast Research in Arabidopsis, R.P. Jarvis, ed (New York: Humana Press), pp. 265–282.

Grimm, B., Dehesh, K., Zhang, L., and Leister, D. (2014). Intracellular communication. Mol. Plant **7:** 1071–1074.

Huang, M., Friso, G., Nishimura, K., Qu, X., Olinares, P.D., Majeran, W., Sun, Q., and van Wijk, K.J. (2013). Construction of plastid reference proteomes for maize and Arabidopsis and evaluation of their orthologous relationships; the concept of orthoproteomics. J. Proteome Res. **12:** 491–504.

Kauss, D., Bischof, S., Steiner, S., Apel, K., and Meskauskiene, R. (2012). FLU, a negative feedback regulator of tetrapyrrole biosynthesis, is physically linked to the final steps of the Mg(++)-branch of this pathway. FEBS Lett. **586:** 211–216.

Kim, J., Kimber, M.S., Nishimura, K., Friso, G., Schultz, L., Ponnala, L., and van Wijk, K.J. (2015). Structures, functions, and interactions of ClpT1 and ClpT2 in the Clp protease system of Arabidopsis chloroplasts. Plant Cell **27:** 1477–1496.

Kim, J., Olinares, P.D., Oh, S.H., Ghisaura, S., Poliakov, A., Ponnala, L., and van Wijk, K.J. (2013). Modified Clp protease complex in the ClpP3 null mutant and consequences for chloroplast development and function in Arabidopsis. Plant Physiol. **162:** 157–179.

Kim, J., Rudella, A., Ramirez Rodriguez, V., Zybailov, B., Olinares, P.D., and van Wijk, K.J. (2009). Subunits of the plastid ClpPR protease complex have differential contributions to embryogenesis, plastid biogenesis, and plant development in Arabidopsis. Plant Cell **21:** 1669–1692.

Kirstein, J., Molière, N., Dougan, D.A., and Turgay, K. (2009). Adapting the machine: adaptor proteins for Hsp100/Clp and AAA+ proteases. Nat. Rev. Microbiol. **7:** 589–599.

Kmiec, B., et al. (2013). Organellar oligopeptidase (OOP) provides a complementary pathway for targeting peptide degradation in mitochondria and chloroplasts. Proc. Natl. Acad. Sci. USA **110:** E3761–E3769.

Lee, U., Rioflorido, I., Hong, S.W., Larkindale, J., Waters, E.R., Vierling, E. (2007). The Arabidopsis ClpB/Hsp100 family of proteins: chaperones for stress and chloroplast development. Plant J. **49:** 115–127.

Liu, K., Ologbenla, A., and Houry, W.A. (2014). Dynamics of the ClpP serine protease: a model for self-compartmentalized proteases. Crit. Rev. Biochem. Mol. Biol. **49:** 400–412.

Moolenaar, G.F., Franken, K.L., Dijkstra, D.M., Thomas-Oates, J.E., Visse, R., van de Putte, P., and Goosen, N. (1995). The C-terminal region of the UvrB protein of *Escherichia coli* contains an important determinant for UvrC binding to the preincision complex but not the catalytic site for 3′-incision. J. Biol. Chem. **270:** 30508–30515.

Moser, J., Schubert, W.D., Heinz, D.W., and Jahn, D. (2002). Structure and function of glutamyl-tRNA reductase involved in 5-aminolaevulinic acid formation. Biochem. Soc. Trans. **30:** 579–584.

Myouga, F., Motohashi, R., Kuromori, T., Nagata, N., and Shinozaki, K. (2006). An Arabidopsis chloroplast-targeted Hsp101 homologue, APG6, has an essential role in chloroplast development as well as heat-stress response. Plant J. **48:** 249–260.

Nishimura, K., Asakura, Y., Friso, G., Kim, J., Oh, S.H., Rutschow, H., Ponnala, L., and van Wijk, K.J. (2013). ClpS1 is a conserved substrate selector for the chloroplast Clp protease system in Arabidopsis. Plant Cell **25:** 2276–2301.

Nishimura, K., and van Wijk, K.J. (2015). Organization, function and substrates of the essential Clp protease system in plastids. Biochim. Biophys. Acta. **1847:** 915–930.

Olinares, P.D., Ponnala, L., and van Wijk, K.J. (2010). Megadalton complexes in the chloroplast stroma of *Arabidopsis thaliana* characterized by size exclusion chromatography, mass spectrometry, and hierarchical clustering. Mol. Cell. Proteomics **9:** 1594–1615.

Ramundo, S., et al. (2014). Conditional depletion of the Chlamydomonas chloroplast ClpP protease activates nuclear genes involved in autophagy and plastid protein quality control. Plant Cell **26:** 2201–2222.

Rivera-Rivera, I., Román-Hernández, G., Sauer, R.T., and Baker, T.A. (2014). Remodeling of a delivery complex allows ClpS-mediated degradation of N-degron substrates. Proc. Natl. Acad. Sci. USA **111:** E3853–E3859.

Rodríguez-Concepción, M., and Boronat, A. (2015). Breaking new ground in the regulation of the early steps of plant isoprenoid biosynthesis. Curr. Opin. Plant Biol. **25:** 17–22.

Rosano, G.L., Bruch, E.M., and Ceccarelli, E.A. (2011). Insights into the Clp/HSP100 chaperone system from chloroplasts of *Arabidopsis thaliana*. J. Biol. Chem. **286:** 29671–29680.

Sauer, K., and Camper, A.K. (2001). Characterization of phenotypic changes in *Pseudomonas putida* in response to surface-associated growth. J. Bacteriol. **183:** 6579–6589.

Sauer, R.T., and Baker, T.A. (2011). AAA+ proteases: ATP-fueled machines of protein destruction. Annu. Rev. Biochem. **80:** 587–612.

Shevchenko, A., Tomas, H., Havlis, J., Olsen, J.V., and Mann, M. (2006). In-gel digestion for mass spectrometric characterization of proteins and proteomes. Nat. Protoc. **1:** 2856–2860.

Shimuta, T.R., Nakano, K., Yamaguchi, Y., Ozaki, S., Fujimitsu, K., Matsunaga, C., Noguchi, K., Emoto, A., and Katayama, T. (2004). Novel heat shock protein HspQ stimulates the degradation of mutant DnaA protein in *Escherichia coli*. Genes Cells **9:** 1151–1166.

Smith, S.C., Joshi, K.K., Zik, J.J., Trinh, K., Kamajaya, A., Chien, P., and Ryan, K.R. (2014). Cell cycle-dependent adaptor complex for ClpXP-mediated proteolysis directly integrates phosphorylation and second messenger signals. Proc. Natl. Acad. Sci. USA **111:** 14229–14234.

Tapken, W., Kim, J., Nishimura, K., van Wijk, K.J., and Pilon, M. (2015). The Clp protease system is required for copper ion-dependent turnover of the PAA2/HMA8 copper transporter in chloroplasts. New Phytol. **205:** 511–517.

Varshavsky, A. (2011). The N-end rule pathway and regulation by proteolysis. Protein Sci. **20:** 1298–1345.

Vizcaíno, J.A., et al. (2014). ProteomeXchange provides globally coordinated proteomics data submission and dissemination. Nat. Biotechnol. **32:** 223–226.

Wandinger, S.K., Richter, K., and Buchner, J. (2008). The Hsp90 chaperone machinery. J. Biol. Chem. **283:** 18473–18477.

Wang, L., Elliott, M., and Elliott, T. (1999a). Conditional stability of the HemA protein (glutamyl-tRNA reductase) regulates heme biosynthesis in *Salmonella typhimurium*. J. Bacteriol. **181:** 1211–1219.

Wang, L., Wilson, S., and Elliott, T. (1999b). A mutant HemA protein with positive charge close to the N terminus is stabilized against heme-regulated proteolysis in *Salmonella typhimurium*. J. Bacteriol. **181:** 6033–6041.

Xiao, Y., Savchenko, T., Baidoo, E.E., Chehab, W.E., Hayden, D.M., Tolstikov, V., Corwin, J.A., Kliebenstein, D.J., Keasling, J.D., and Dehesh, K. (2012). Retrograde signaling by the plastidial metabolite MEcPP regulates expression of nuclear stress-response genes. Cell **149:** 1525–1535.

Yang, J., Yan, R., Roy, A., Xu, D., Poisson, J., and Zhang, Y. (2015). The I-TASSER Suite: protein structure and function prediction. Nat. Methods **12:** 7–8.

Zeth, K., Ravelli, R.B., Paal, K., Cusack, S., Bukau, B., and Dougan, D.A. (2002). Structural analysis of the adaptor protein ClpS in complex with the N-terminal domain of ClpA. Nat. Struct. Biol. **9:** 906–911.

Zhang, M., Zhang, F., Fang, Y., Chen, X., Chen, Y., Zhang, W., Dai, H.E., Lin, R., and Liu, L. (2015). The non-canonical tetratricopeptide repeat (TPR) domain of fluorescent (FLU) mediates complex formation with glutamyl-tRNA reductase. J. Biol. Chem. **290:** 17559–17565.

Zhao, A., Fang, Y., Chen, X., Zhao, S., Dong, W., Lin, Y., Gong, W., and Liu, L. (2014). Crystal structure of Arabidopsis glutamyl-tRNA reductase in complex with its stimulator protein. Proc. Natl. Acad. Sci. USA **111:** 6630–6635.

Zybailov, B., Friso, G., Kim, J., Rudella, A., Rodríguez, V.R., Asakura, Y., Sun, Q., and van Wijk, K.J. (2009). Large scale comparative proteomics of a chloroplast Clp protease mutant reveals folding stress, altered protein homeostasis, and feedback regulation of metabolism. Mol. Cell. Proteomics **8:** 1789–1810.